All-Polymer Bistable Resistive Memory Device Based on Nanoscale Phase-Separated PCBM-Ferroelectric Blends

*M. A. Khan, Unnat S. Bhansali, Dongkyu Cha, and H. N. Alshareef**

All polymer nonvolatile bistable memory devices are fabricated from blends of ferroelectric poly(vinylidenefluoride–trifluoroethylene (P(VDF-TrFE)) and n-type semiconducting [6,6]-phenyl-C61-butyric acid methyl ester (PCBM). The nanoscale phase separated films consist of PCBM domains that extend from bottom to top electrode, surrounded by a ferroelectric P(VDF-TrFE) matrix. Highly conducting poly(3,4-ethylenedioxythiophene):poly(styrenesulfonate) (PEDOT:PSS) polymer electrodes are used to engineer band offsets at the interfaces. The devices display resistive switching behavior due to modulation of this injection barrier. With careful optimization of the solvent and processing conditions, it is possible to spin cast very smooth blend films ($R_{rms} \approx 7.94$ nm) and with good reproducibility. The devices exhibit high I_{on}/I_{off} ratios ($\approx 3 \times 10^3$), low read voltages ($\approx$5 V), excellent dielectric response at high frequencies ($\varepsilon_r \approx 8.3$ at 1 MHz), and excellent retention characteristics up to 10 000 s.

1. Introduction

Polymer-based resistive memories targeting next-generation transparent and flexible electronics are experiencing unprecedented levels of research activity. They are promising circuit elements due to their simple device structure, easy processability, high storage density, and the potential they offer for large-area and low-cost, large-area deposition techniques such as spin coating, roll-to-roll processing, and ink jet printing.[1] Among polymer memories, fullerene-based composites have been studied for their write once read many (WORM) memory behavior. Most of these systems are reported to work by either charge trapping or charge transfer mechanism.[2–5] Aggregation of fullerene leading to electrical shorts and unstable memory behavior remains a significant problem. Therefore, the development of fullerene-based nonvolatile memory devices is still in its early stages. On the other hand, ferroelectric memories based on the copolymer poly(vinylidenefluoride–trifluoroethylene) [P(VDF-TrFE)] have been widely studied and are of particular interest to the organic electronics community due to its nonvolatility, large spontaneous polarization, excellent chemical stability, and low temperature processability.[6]

M. A. Khan, Dr. U. S. Bhansali, Dr. D. Cha, Prof. H. N. Alshareef
King Abdullah University of Science and Technology (KAUST)
Thuwal 23955-6900, Saudi Arabia
E-mail: husam.alshareef@kaust.edu.sa

DOI: 10.1002/adfm.201202724

Ferroelectric capacitor memories make use of the hysteresis behavior by associating +Pr and –Pr states with Boolean 1 and 0 logic states. The problem with using ferroelectric capacitors is that they suffer from destructive read-out, as the voltage applied to read the information can erase it as well.[7] Ferroelectric transistor (FeFETs) memories solve this problem as they provide resistive switching that can be sampled at low voltages without affecting the ferroelectric polarization. Historically, polymer FeFETs have suffered from poor performance due to low mobilities, low ON/OFF ratios, poor retention characteristics and high operating voltages. Surface roughness, defects and leakage through the P(VDF-TrFE) film are some of the reasons for the poor performance.[6,7] Further, FeFETs are a complicated three terminal device making it difficult to scale up to an integrated memory circuit. Recently Asadi et al. demonstrated a breakthrough device using phase-separated films of P(VDF-TrFE) and the p-type polymer semiconductor rir-P3HT [regio-irregular poly(3-hexylthiophene)].[8] The proposed working principle in these devices is that the dipole alignment in the ferroelectric component of the blend modulates the injection barrier at the semiconductor–electrode interface. These polymer blend devices, which used only metal electrodes, have a simple two terminal structure like a capacitor and at the same time provide resistive switching like the FeFETs. The choice of semiconductor material and electrode becomes very critical in order to engineer an injection barrier at the interface. This is necessary to achieve current modulation in these devices. p-type semiconductors such as rir-P3HT and phenyl-substituted poly(phenylene-vinylene) (SY) with highest occupied molecular orbital (HOMO) levels of 5.1 and 5.4 eV, respectively form an injection barrier with metal electrodes like Ag and Al with work functions of 4.3 and 4.2 eV, respectively.[9] On the other hand, they form ohmic contacts with polymer electrodes like PEDOT: PSS (poly(3,4-ethylenedioxythiophene):poly(styrenesulfonate); work function of 5.1 eV), which is undesirable to obtain resistive switching. Furthermore, blends of these p-type semiconductors and ferroelectric P(VDF-TrFE) suffer from coarse phase separation resulting in high surface roughness leading to electrical shorts and low device yields as reported in the work by Asadi et al.[10]

In this study, we have fabricated the first resistive memory devices based on n-type semiconductor-ferroelectric polymer blends and optimized their performance. Our devices are all-polymer, non-volatile, bi-stable, resistively switched, and

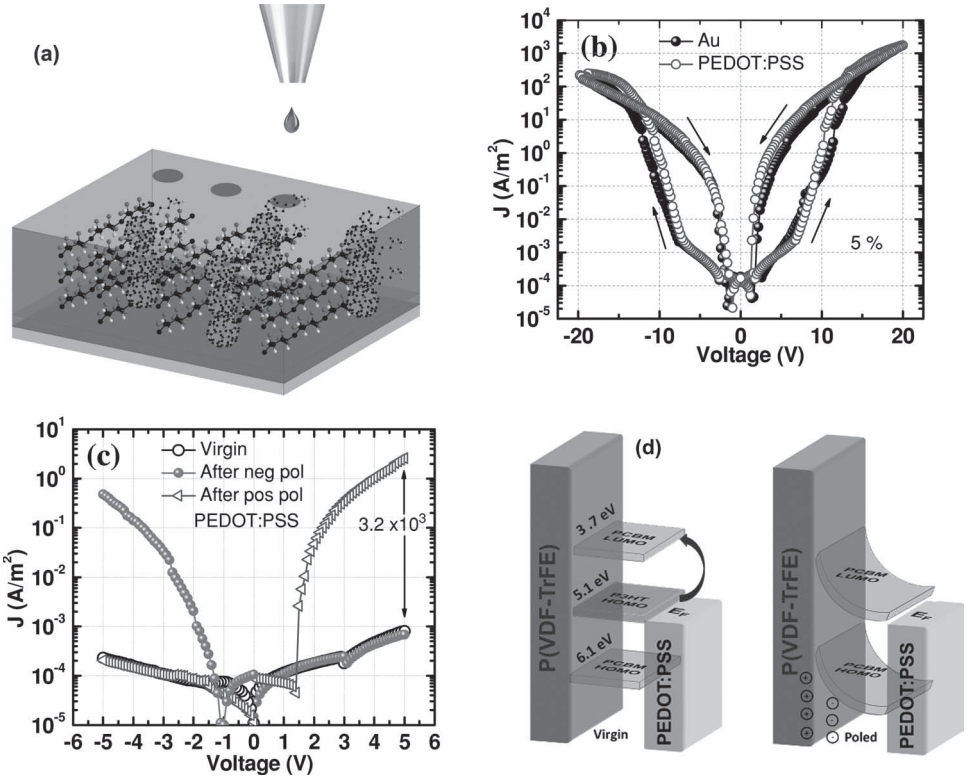

Figure 1. a) Schematic 3D cross section of all polymer memory devices with phase separated network of P(VDF-TrFE) and PCBM polymers. PEDOT:PSS was ink-jet printed as the top electrode. b) Current density–voltage (*J–V*) sweeps of P(VDF-TrFE)-PCBM blend (95:5) devices with Au and PEDOT:PSS electrodes showing resistive memory behavior. c) *J–V* memory performance of virgin polymer P(VDF-TrFE)-PCBM blends (95:5) and after positive and negative poling. d) Band diagram at the interface between PCBM phase and bottom PEDOT:PSS electrode for virgin and poled devices.

incorporate nanoscale phase separated blends of a ferroelectric and semiconducting material. Highly conducting PEDOT:PSS polymer electrodes are used to engineer the band offsets at the interfaces. By carefully optimizing the solvent and processing conditions we achieved very smooth films with low surface roughness (R_{rms} ≈ 7.94 nm) and good reproducibility. The devices exhibit high I_{on}/I_{off} ratios (≈3×10^3), low read voltages (≈5 V), excellent dielectric response at high frequencies ($\varepsilon_r \approx 8.3$ at 1 MHz) and excellent retention characteristics up to 10 000 s.

2. Results and Discussion

2.1. Switching behavior of Blend films

A schematic of the all-polymer resistive memory device with highly conducting top and bottom PEDOT:PSS electrodes ($\sigma \approx$ 900 S/cm) is shown in **Figure 1**a. The active single-layer consists of a film spin cast from a blend of ferroelectric P(VDF-TrFE) and n-type semiconducting PCBM ([6,6]-phenyl-C61-butyric acid methyl ester) from a common solvent - cyclohexanone. The active layer consists of an interpenetrating network of the P(VDF-TrFE) matrix (70–30 molar ratio) with the semiconducting PCBM phase forming continuous channels between the two polymer electrodes, a feature that is essential for the operation of these devices. Device fabrication details are discussed in the experimental section of the manuscript. Highly conducting doped PEDOT:PSS top electrodes ($\sigma \approx$ 900 S/cm) with an area of approx. 7.85×10^{-5} cm^2, were ink-jet printed on top of the phase separated blend films. The processing was optimized for different blend ratios from 1 to 15 wt% PCBM. Devices with 10 wt% and higher PCBM content suffered from high leakage leading to low device yields. The best performance and yield were achieved using devices with 5 wt% PCBM content.

Figure 1b shows the current density–voltage (*J–V*) characteristics of 200-nm-thick blend films of ferroelectric P(VDF-TrFE) containing 5 wt% n-type semiconductor (PCBM). The *J–V* curves of the devices show a current hysteresis on both positive and negative sweeps from 0 to 20 V and 0 to –20 V, indicative of a bistable nonvolatile resistive memory device. The device can be programmed into high and low resistance states (OFF/ON) by applying a voltage pulse larger than the coercive field of the ferroelectric (≈±20 V). These nonvolatile memory devices can be read out non-destructively at low bias unlike ferroelectric capacitors which suffer from a destructive read-out. Devices fabricated on both Au and PEDOT:PSS electrodes showed similar hysteresis loops. This is expected due to the similar work function of Au (≈5.1 eV) and HOMO level of PEDOT:PSS (≈5 eV).[11] Switching behavior for P(VDF-TrFE) ≈5 wt% PCBM blends sandwiched between polymeric PEDOT:PSS electrodes is shown in Figure 1c. For all switching characterization, the

bottom electrode was grounded and the bias applied to the top electrode. At low positive biases (0 to 5 V) less than the coercive field of the P(VDF-TrFE), the charge injection is from the bottom electrode interface. In the virgin unpoled state, the current is low (≈10^{-3} A/m^2) due to the large injection barrier between the PEDOT:PSS and the PCBM. Figure 1d shows the band diagram at the bottom interface between the bottom PEDOT:PSS electrode, ferroelectric P(VDF-TrFE) and semiconducting PCBM. The mismatch of HOMO of PEDOT:PSS (≈5 eV) and the lowest unoccupied molecular orbital (LUMO) level of n-type PCBM (3.7 eV) forms a large injection barrier (≈1.3 eV) for charge carriers.[12] Thus, there is poor charge injection and the current is low. This is unlike previously reported p-type semiconductors like P3HT which form an ohmic contact with PEDOT: PSS.[9] Without having the injection barrier between the electrode and semiconducting phase, the device is always in a low resistance state (ON) and cannot be turned OFF. Subsequently, the ferroelectric is poled with a positive bias (+20 V) at the top electrode as shown in the poled band diagram on the right in Figure 1d. The dipoles in the ferroelectric phase rotate and align with the electric field. Due to the alignment of dipoles, negative polarization charge is built up in the P(VDF-TrFE) phase at the interface with the top electrode, while positive polarization charge accumulates at the interface with bottom electrode. To neutralize the positive polarization charge, negative charges accumulate in the n-type PCBM semiconductor at the interface with the bottom electrode. The accumulated charge leads to a strong band bending in the PCBM phase, effectively reducing the injection barrier at the bottom electrode. This is indicated by poled band diagram in Figure 1d (positively poled case), showing the lowering of the injection barrier. Subsequent sweeps up to a low bias, +5 V see efficient injection of charges due to lack of an injection barrier. This current density is more than 3 orders of magnitude larger than the virgin unpoled junction, thus turning the device ON. When the device is poled with an opposite polarity i.e., negative bias (–20 V) applied at the top electrode, the negative polarization charge in P(VDF-TrFE) at the bottom interface builds up. The negative charge polarization cannot be compensated by the n-type PCBM. Thus injection barrier remains constant at bottom interface and the device goes back to an OFF state like the virgin unpoled state. Thus the interface is bistable and can be switched to an ON and OFF state by poling with opposite polarity voltage pulses. Similarly at reverse bias, where charges have to be injected at the top interface the device can be turned into ON and OFF states, as seen in Figure 1c. Thus the devices exhibit nonvolatile bistable resistive memory behavior with excellent yields and a small spread in current densities.

2.2. Physical Characterization of Blend films

2.2.1. Morphology

The morphology of the blend films is very critical to achieving nonvolatile resistive switching memory behavior in these devices as explained above. **Figure 2**a is a TEM cross section that shows the morphology of these polymer blend films with 5 wt% PCBM sandwiched between gold electrodes. The morphology of these blend films consists of phase separated semiconducting PCBM domains that extend from bottom to top electrode, surrounded by a ferroelectric P(VDF-TrFE) matrix. The observed phase separation was seen in multiple locations throughout the film, as shown in Figure 2b with an average width of the PCBM phase between 80–90 nm. Figure 2c shows the chemical structure of ferroelectric copolymer, P(VDF-TrFE) [$(\text{-CH}_2\text{-CF}_2\text{-})_n$-$(\text{CHFCF}_2)_m$] and n-type semiconducting PCBM [$C_{72}H_{14}O_2$]. The ferroelectricity of PVDF stems from the dipole moments in the molecule that can be aligned with the applied field by rotation of the polymer chain. The dipole moments originate predominantly from the presence of the strongly electronegative fluorine atoms and electropositive hydrogen.[1] Figure 2d shows high resolution X-ray elemental mapping of the polymer blend film using EFTEM (Energy filtered TEM). Based on the presence of fluorine in P(VDF-TrFE), the images clearly distinguish the phase separated P(VDF-TrFE) matrix (red) with the semiconducting PCBM phase (black) which is continuous between the two electrodes.

The surface morphology and grain growth of 200-nm-thick polymer blend films annealed at 135 °C was characterized using atomic force microscopy (AFM). The surface topography images of pure ferroelectric P(VDF-TrFE) i.e., 0 wt% PCBM and blends with 5 wt% PCBM and 10 wt% PCBM are shown in **Figure 3**a–c, respectively. The measured surface roughness of our PCBM blend films surprisingly shows very smooth films with R_{rms} of ≈7.94 nm and 11.5 nm for 5 wt% and 10 wt% films, respectively. The surface roughness is comparable to the pure P(VDF-TrFE) films which have an average R_{rms} ≈ 6.9 nm. This is a remarkable improvement from previous reports on ferroelectric-semiconductor blend films of P(VDF-TrFE) and rir-P3HT where the coarse phase separation leads to surface roughness ≈100 nm comparable to film thickness.[9,10] High surface roughness leads to nonuniform electrical field across the active layer and possibly poor yield and reproducibility. Previous studies have used tetrahydrofuran (THF) as a common solvent for both P(VDF-TrFE) and P3HT[10], but is a poor solvent for both. P3HT has poor solubility in THF while its low viscosity (0.456 mPa s at 25 °C), low boiling point (66 °C) and high vapor pressure (143 mmHg at 20 °C) are detrimental to P(VDF-TrFE) film forming characteristics. The use of cyclohexanone, a common solvent that dissolves the ferroelectric and semiconductor material is key to obtaining extremely smooth films resulting in high performance and yields for our devices. Cyclohexanone has recently been reported in spin-cast ultra-thin and smooth P(VDF-TrFE) films.[13] It has a high solubility for P(VDF-TrFE) and its high boiling point (156 °C), viscosity (2 mPa s at 25 °C) and vapor pressure (5 mmHg at 25 °C) make it an excellent solvent for spin casting ferroelectric P(VDF-TrFE) thin films. At the same time it also has an excellent solubility for PCBM (>91%).[14] Using cyclohexanone we were able to make clear homogeneous solutions of P(VDF-TrFE) and PCBM even at high concentrations of PCBM (>10 wt%), as seen from the photograph in **Figure 4**a. Thus, we were able to fabricate very smooth blend films, with a drastic improvement in roughness to previous reports. Any small fluctuations in the homogeneity of the solution will lead to coarse phase separation and rough films.

The AFM phase images in Figure 3d–f show the P(VDF-TrFE) grains in a pure ferroelectric film, 5 wt% PCBM and

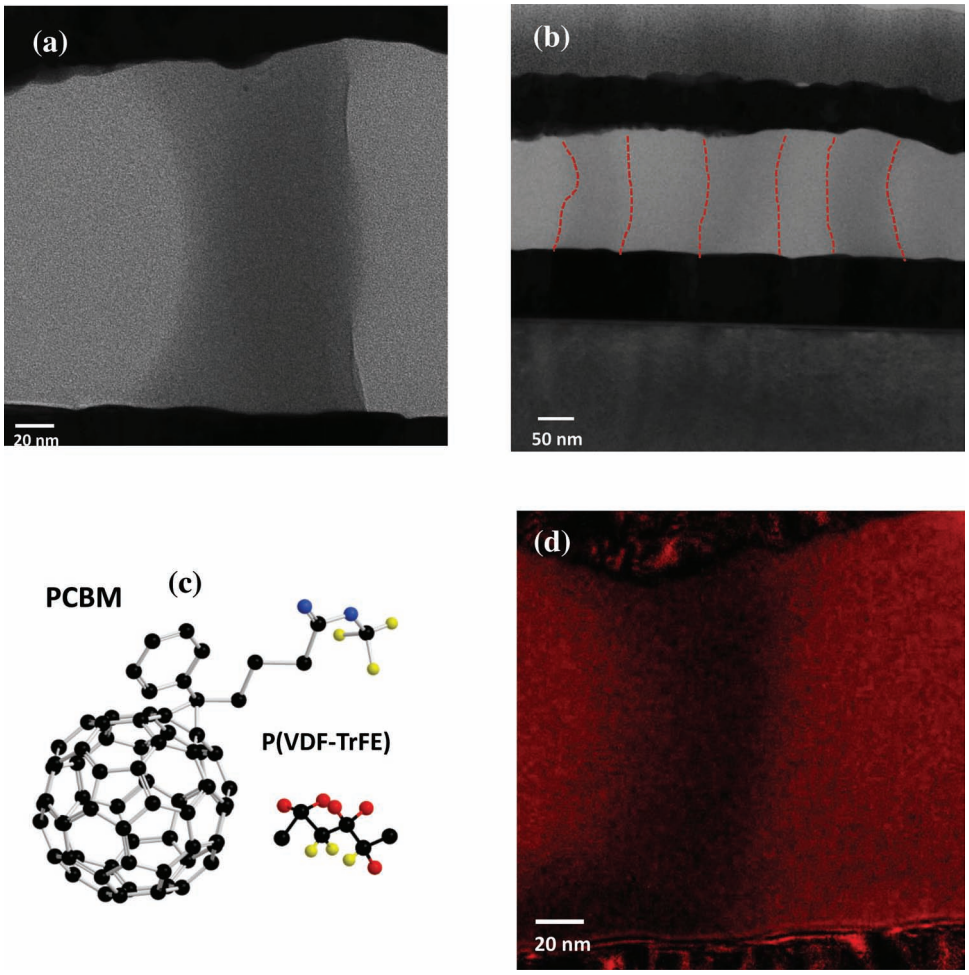

Figure 2. a) Cross section TEM showing nanometer-scale phase separated PCBM continuously between the gold electrodes. b) Cross section TEM showing multiple phase-separated PCBM columns throughout the thin film with an average domain width of ≈80 nm. The red lines are a visual aid for delineation of the PCBM phase in the PVDF TrFE matrix. c) Molecular structures of semiconducting PCBM (left) and ferroelectric P(VDF-TrFE) (right). d) X-ray elemental mapping of the polymer blend film using EFTEM showing the fluorine (red) in the P(VDF-TrFE) phase.

10 wt% PCBM, respectively. The average grain size of pure P(VDF-TrFE) is approximately 200 nm, consistent with previous reports in literature and indicating high crystallinity.[1,6] Polymer blend films with 5 and 10 wt% PCBM also show well crystallized P(VDF-TrFE) grains with an average grain size of ≈160 and 150 nm respectively. We believe the addition of PCBM leads to an increase in nucleation site density leading to smaller grain size observed for P(VDF-TrFE).

A photograph of the solutions and the all polymer memory devices with 0, 5, and 10 wt% PCBM composition is shown in Figure 4a. Cyclohexanone forms a clear homogenous viscous solution with P(VDF-TrFE) and PCBM even at high concentrations. This is very critical in getting smooth polymer blend films essential for good device performance, as explained above. Figure 4b shows the UV-vis optical transmission spectra of P(VDF-TrFE)-PCBM blends films spun on glass substrates. At approximately $\lambda = 600$ nm, bare glass substrates have transmission up to ≈87% and the transmission drops to ≈70 and 60% for 5 and 10 wt% PCBM devices, respectively.

2.2.2. Crystal Structure and Orientation

Figure 5a shows the Grazing Incidence X-ray diffraction (GIXRD) spectra which was used to study the crystal structure of pure ferroelectric P(VDF-TrFE) and the polymer blends with PCBM. Pristine P(VDF-TrFE) films spun on PEDOT:PSS electrodes and annealed at 135 °C exhibit a peak centered at $2\theta \approx 19.85°$, characteristic of the ferroelectric β phase and reflection from the (110) and (200) planes. The inter-planar distance was calculated to be approximately 4.46 Å and is consistent with earlier reports.[15] In comparison, the blend films exhibit a peak slightly shifted to the left at $2\theta \approx 19.75°$ and 19.6° for 5 and 10 wt% PCBM films, respectively indicating a larger interplanar distance. It is possible that with increasing PCBM content, some of the PCBM molecules are intercalating between the P(VDF-TrFE) polymer chains leading to larger interplanar distance. Furthermore, the XRD peaks indicate that the polymer blend films have smaller crystallite size compared to the pristine P(VDF-TrFE) films with a larger full-width-half-maximum (FWHM), as confirmed by the AFM images above.

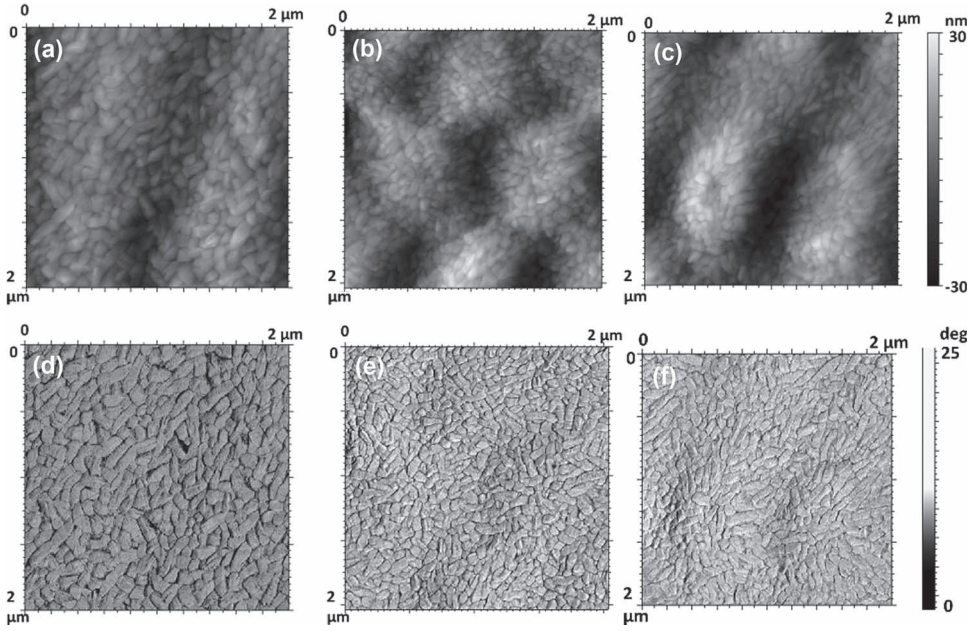

Figure 3. AFM images showing topography (a,b,c) and phase (d,e,f) images of a blend with 0, 5, and 10 wt% PCBM, respectively. Surface roughness (R_{rms}) ≈ 6.9, 7.94, and 11.5 nm for 0, 5, and 10 wt% PCBM films.

The presence of PCBM in thin films of the polymer blend was verified using transmission mode Fourier transform infrared (FTIR) spectroscopy. Figure 5b shows the absorbance bands at 1288 and 850 cm^{-1} associated with CF_2 symmetric stretching vibration and are characteristic bands of the trans-zigzag formation (β phase).[15–17] Other major peaks identified are the 1400 cm^{-1} band characteristic of the CH_2 wagging vibrations, 1186 cm^{-1} band characteristic of asymmetric stretching of CF_2 and the 880 cm^{-1} band related to the rocking CH_2 vibration.[16] All these peaks were common in both pristine P(VDF-TrFE) and PCBM blended films. A couple of extra peaks were identified in the blend films at 1246 cm^{-1} characteristic of O=C–O–C stretching and at 1124 cm^{-1} from C–O–C stretching from the methyl ester group in the PCBM.[18] FTIR analysis proves the presence of PCBM in these polymer blend films but does not suggest any interaction or bonding between the PCBM and P(VDF-TrFE) chains.

2.3. Device Characterization of Blend Films

Figure 6a shows the *J–V* characteristics of 200-nm-thick pure ferroelectric P(VDF-TrFE) film. The *J–V* curves of pre-poled devices show no current hysteresis on either positive or negative bias sweeps and is consistent with the leakage current behavior of P(VDF-TrFE). At the same time *J–V* loops for un-annealed blend films with 5 wt% PCBM, show negligible hysteresis. This indicates that the current hysteresis and the resistive switching in blend films arise due to the ferroelectric polarization which modulates the current injection into the PCBM phase.

Ferroelectric hysteresis of pure P(VDF-TrFE) capacitors with a remnant polarization (P_r) of 7.1 µC/cm^2 and coercive field (E_c) of ≈ 50 MV/m is shown in Figure 6b. The polarization could not be measured for P(VDF-TrFE) and PCBM blends even though FTIR and XRD analysis indicate the presence of ferroelectric β phase. This might be due to the high leakage current through the PCBM phase at high fields used for the P-V measurement. Small signal capacitance–voltage (*C–V*) curves measured by superimposing a small AC electric field (100 mV, 1 MHz) over DC field sweep are also shown in Figure 6b. It is a measure of the modulation of dielectric constant by the remanent polarization state. The 200-nm-thick P(VDF-TrFE)-PCBM blend films display a peak capacitance of ≈35 nF/cm^2,

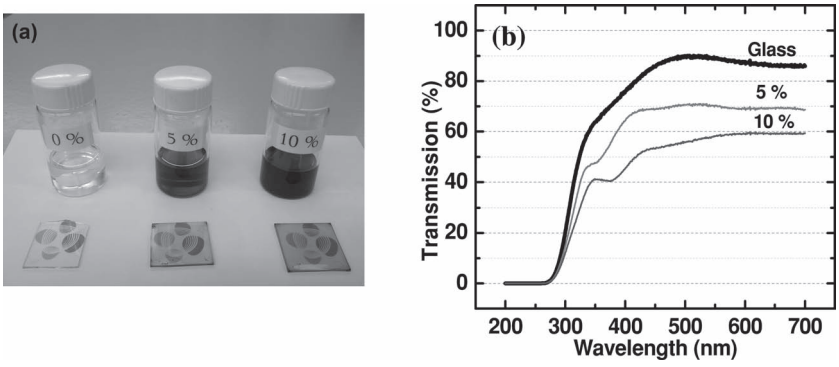

Figure 4. a) Photographs of the all-polymer transparent nonvolatile resistive memory fabricated on glass substrates. The corresponding solutions with 0, 5, and 10 wt% PCBM (left to right) showing a homogenous solution. b) UV-vis transmission spectra for devices with 5 and 10 wt% PCBM blend films.

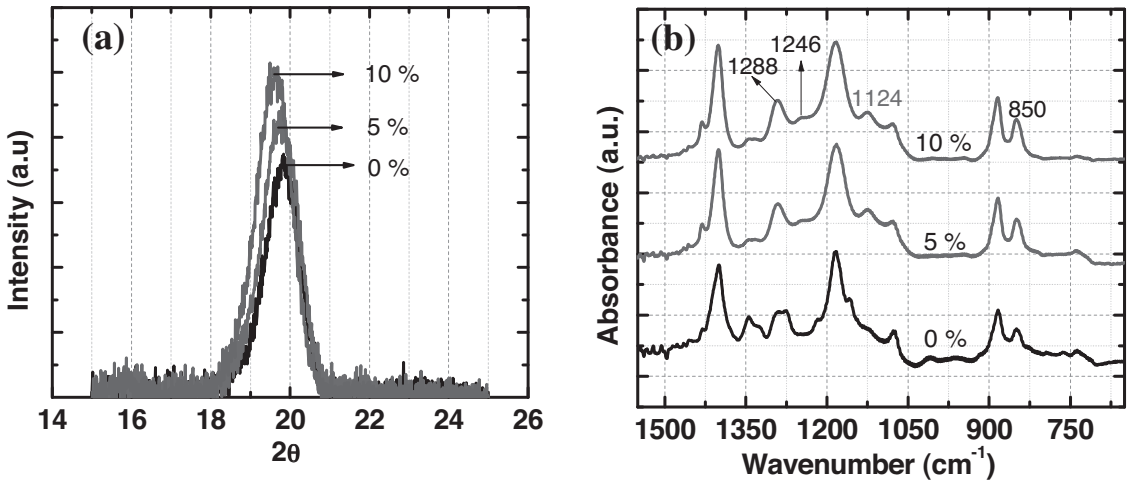

Figure 5. a) Grazing incidence XRD spectra for pure ferroelectric P(VDF-TrFE) and blend films with 5 and 10 wt% PCBM. b) FT-IR spectra of pure ferroelectric P(VDF-TrFE) and 5 and 10 wt% PCBM blend thin films.

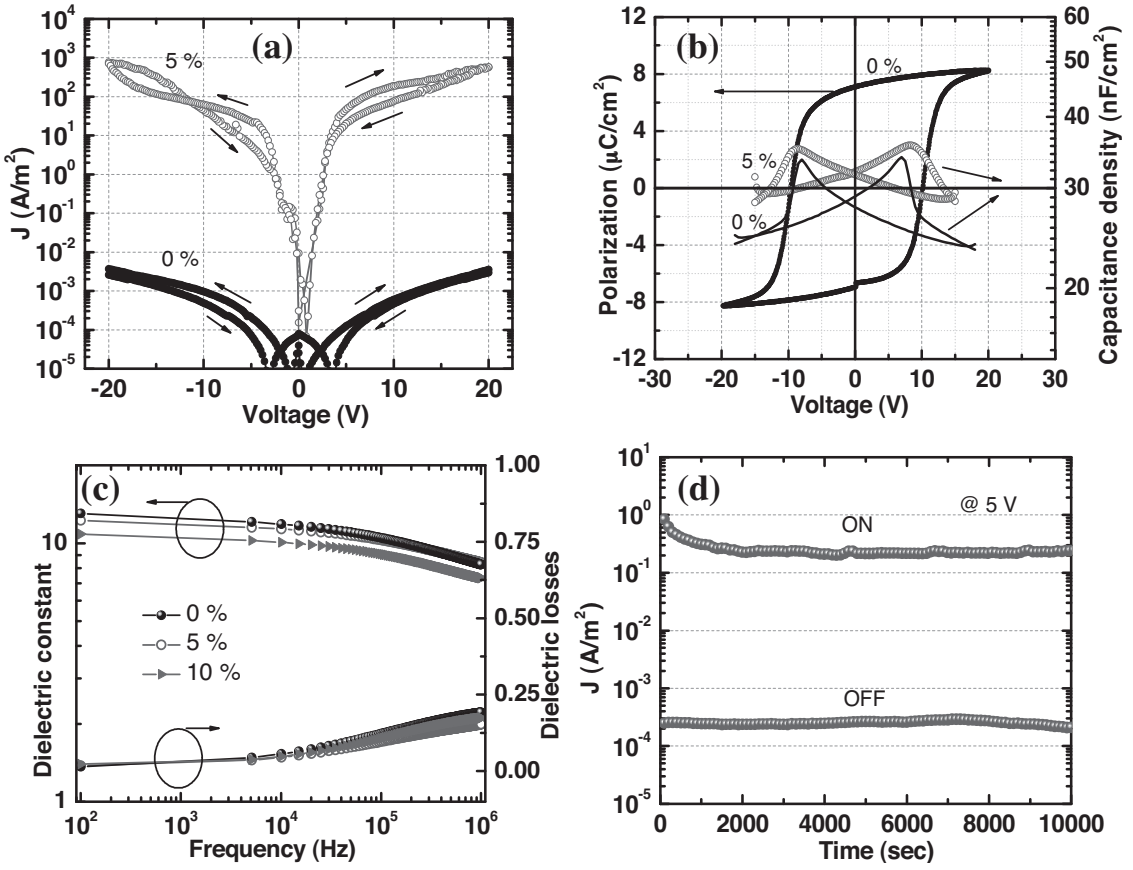

Figure 6. a) Current density–voltage characteristics of 200-nm pure P(VDF-TrFE) films showing no current hysteresis. Unannealed 5 wt% polymer blend films show an increase in current by 5 orders of magnitude but no memory behavior. b) Polarization-voltage hysteresis curve for 200-nm, pure ferroelectric films at 10 Hz (left axis). Small signal capacitance–voltage (butterfly loops) at (100 mV,1 MHz) for pure P(VDF-TrFE) films and blends with 5 wt% PCBM (Right axis). c) Dielectric spectroscopy study with dielectric constant (left axis) and dielectric losses (right axis) for pure ferroelectric P(VDF-TrFE) (0 wt% PCBM) and polymer blend films with 5 and 10 wt% PCBM content. d) Retention characteristics of nonvolatile resistive memory with 5 wt% PCBM measured at $V = +5$ V showing an ON/OFF ratio of $\approx 10^3$. A voltage pulse of +20 V and −20 V was applied to turn the device ON or OFF, respectively, before the test.

comparable to pure P(VDF-TrFE) devices. A characteristic "butterfly" shape of the *C–V* curve is seen for blends with 5 wt% PCBM content, typical for ferroelectric materials. Figure 6c shows the dielectric dispersion and the loss factor (tan δ) of pure P(VDF-TrFE) and blend memory devices. A gradual decay of the dielectric constant is observed, consistent with the dielectric response of ferroelectric thin films. Our P(VDF-TrFE) copolymer films exhibit a dielectric constant of ≈12.9 at 100 Hz, comparable to other reports in literature.[19] Upon adding PCBM the dielectric permittivity does not change as the response is dominated by the ferroelectric phase in the blend films. Devices with 5 wt% PCBM and 10 wt% PCBM also show excellent frequency dispersion up to frequencies of 1 MHz, with a negligible drop in permittivity and low losses.

Data retention characteristics of our devices were examined by a measurement of the current as a function of time. Figure 6d shows the value of current density in the ON and OFF states as a function of retention time, measured at 5 V. The ON and OFF states were produced at by poling the device at +20 and –20 V, respectively. The all-polymer nonvolatile bistable resistive memory devices show excellent retention with the ON/OFF ratio of three orders of magnitude even after 10 000 s, with almost no change in current modulation.

3. Conclusion

In summary, we have fabricated all-polymer nonvolatile bistable resistive memory devices made from phase separated blends of ferroelectric P(VDF-TrFE) and n-type semiconducting PCBM. The ferroelectric polarization modulated the current injection into the semiconducting phase, thus controlling the resistive switching behavior. The use of an n-type semiconductor helps us to fabricate an all-polymer device. Coarse phase separation of such polymer blend films has been an issue in the past. This leads to large surface roughness and low device yields. The use of a cyclohexanone as a common solvent which has excellent solubility to both P(VDF-TrFE) and PCBM helped us fabricate devices with very low surface roughness (R_{rms} ≈ 7.94 nm) leading to good device yields. Our devices demonstrate excellent performance with low read voltages (≈5 V), good ON/OFF ratio (≈3×10^3), low frequency dispersion (upto 10^6 Hz) and long retention times of more than 10 000 s. The all-polymer, cost effective, solution processed devices are fabricated at low temperatures and have excellent performance comparable to devices with metal electrodes. This opens up the possibility of large scale fabrication of these resistive memory devices for flexible and transparent electronic applications.

4. Experimental Section

Sample Preparation: The resistive memory devices with P(VDF-TrFE):PCBM blend films were fabricated on transparent glass substrates. Prior to device fabrication, the substrate was cleaned by a sequence of ultrasonication in acetone, isopropanol followed by deionized water. The glass substrates were then treated with O_2 plasma at a low RF power (≈10 W) and pressure of 150 mTorr for 2 min, rendering the surface hydrophilic. PEDOT:PSS in the form of Clevios PH-1000 from Heraeus was chemically doped with ≈4% dimethylsulfoxide (DMSO) to achieve maximum conductivity of ≈900 S/cm. Bottom electrodes were formed by spinning the doped PEDOT:PSS solutions at 1500 rpm for 30 s followed by annealing on a hotplate at 120 °C for 30 min. Simultaneously, as the bottom electrode, 80 nm Au was evaporated using e-beam onto silicon substrates, with an 8-nm Ti adhesion layer.

High purity (99.8%) cyclohexanone (Acros) was used as the common solvent for both the ferroelectric copolymer P(VDF–TrFE) and the n-type organic semiconductor PCBM. P(VDF-TrFE) (70–30 mol%) obtained from Piezotech S.A, France was dissolved in cyclohexanone at a concentration of 30 mg/mL of P(VDF–TrFE) for a pure ferroelectric layer. A 5% PCBM solution was prepared by adding 15.78 mg of PCBM to 300 mg P(VDF-TrFE) and dissolved at 50 °C for 24 h. Similarly solutions with different concentrations of PCBM (3%, 7%, 10%, and 15%) were prepared by varying the amount of PCBM (9.27, 22.58, 33.33, and 52.94 mg), added to 300 mg of P(VDF-TrFE). All the different concentrations of PCBM formed clear homogenous solutions stable even after a few weeks. The filtered polymer blend films were spun in a nitrogen filled glove box, at 3000 rpm for 60 s followed by a soft bake for 30 min at 90 °C. The films were then annealed in vacuum at 135 °C for 4 h to improve the crystallinity of the P(VDF-TrFE) phase. The thickness of the films was ≈200 ± 20 nm as measured by a Dektak profilometer, and did not change with increasing PCBM concentrations. Finally a drop-on-demand piezoelectric inkjet-printing technique using a Jetlab II Precision Printing Platform (Microfab Technologies, Inc.) was used to print the top PEDOT:PSS electrodes. Devices with Au top electrodes were completed by thermally evaporating ≈60 nm Au through a shadow mask.

Characterization: All current-voltage measurements were carried out in air ambient using Keithley 4200 semiconductor characterization system. Transmission data for the polymer blend films were obtained using UV-vis optical absorption spectra (ThermoScientific Evolution 600). Surface morphology and roughness for films was studied using atomic force microscopy (Agilent 5400). Cross section morphology of the devices was studied using transmission electron microscopy (Titan ST) and operated at an accelerating voltage of 300 kV. Energy filtered TEM analysis was done to elementally map fluorine in the polymer blend films. The crystallinity and inter-planar distance of polymer chains was evaluated using grazing incidence X-ray diffraction (Bruker D8 Discover) while the bonding and dipole orientation was analyzed using Fourier-transform infrared spectroscopy (FT-IR, ThermoScientific Nicolet iS10).

Acknowledgements

The authors acknowledge the generous financial support from the KAUST baseline fund and Saudi Basic Industries (SABIC) Grant No. 2000000015. The authors also acknowledge Mrs. Supriya Chewle for her help with artistic rendering of the images.

Received: September 19, 2012
Published online: November 21, 2012

[1] Q.-D. Ling, D.-J. Liaw, C. Zhu, D. S.-H. Chan, E.-T. Kang, K.-G. Neoh, *Prog. Polym. Sci.* **2008**, *33*, 917.
[2] J. Liu, Z. Yin, X. Cao, F. Zhao, A. Lin, L. Xie, Q. Fan, F. Boey, H. Zhang, W. Huang, *ACS Nano* **2010**, *4*, 3987.
[3] S. G. Hahm, N.-G. Kang, W. Kwon, K. Kim, Y.-G. Ko, S. Ahn, B.-G. Kang, T. Chang, J.-S. Lee, M. Ree, *Adv. Mater.* **2012**, *24*, 1062.
[4] J.-C. Hsu, C.-L. Liu, W.-C. Chen, K. Sugiyama, A. Hirao, *Macromol. Rapid. Commun.* **2011**, *32*, 528.
[5] M. H. Lee, D. Y. Yun, H. M. Park, T. W. Kim, *Appl. Phys. Lett.* **2011**, *99*, 183301.
[6] Y. J. Park, I.-s. Bae, S. J. Kang, J. Chang, C. Park, *IEEE Trans. Dielectr. Electr. Insul.* **2010**, *17*, 1135.
[7] R. C. G. Naber, K. Asadi, P. W. M. Blom, Dago M. de Leeuw, B. d. Boer, *Adv. Mater.* **2010**, *22*, 933.

[8] K. Asadi, D. M. D. Leeuw, B. D. Boer, P. W. M. Blom, *Nat. Mater.* **2008**, *7*, 547.
[9] K. Asadi, T. G. D. Boer, P. W. M. Blom, D. M. D. Leeuw, *Adv. Funct. Mater.* **2009**, *19*, 3173.
[10] K. Asadi, H. J. Wondergem, R. S. Moghaddam, C. R. McNeill, N. Stingelin, B. Noheda, P. W. M. Blom, D. M. D. Leeuw, *Adv. Funct. Mater.* **2011**, *21*, 1887.
[11] J.-S. Yeo, J.-M. Yun, D.-Y. Kim, S. Park, S.-S. Kim, M.-H. Yoon, T.-W. Kim, S.-I. Na, *ACS Appl. Mater. Interfaces* **2012**, *4*, 2551.
[12] J. J. Benson-Smith, L. Goris, K. Vandewal, K. Haenen, J. V. Manca, D. Vanderzande, D. D. C. Bradley, a. J. Nelson, *Adv. Funct. Mater.* **2007**, *17*, 451.
[13] R. C. Naber, B. d. Boer, P. W. Blom, D. M. d. Leeuw, *Appl. Phys. Lett.* **2005**, *87*, 203509.
[14] J.-H. Kim, J. H. Park, J. H. Lee, J. S. Kim, M. Sim, C. Shima, K. Cho, *J. Mater. Chem.* **2010**, *20*, 7398.
[15] M. A. Khan, U. S. Bhansali, H. N. Alshareef, *Org. Electron.* **2011**, *12*, 2225.
[16] A. A. Prabu, K. J. Kim, C. Park, *Vib. Spectrosc.* **2009**, *49*, 101.
[17] N. M. Reynolds, K. J. Kim, C. Chang, S. L. Hsu, *Macromolecules* **1989**, *22*, 1092.
[18] H. B. Yildiz, S. Kiralp, L. Toppare, F. Yilmaz, Y. Yagci, K. Ito, T. Senyo, *Polym. Bull.* **2005**, *53*, 193.
[19] M. A. Khan, U. S. Bhansali, H. N. Alshareef, *Adv. Mater.* **2012**, *24*, 2165.